Arab Remote Sensing and Geographic Information System Organisation

Use Remote Sensing To Map Soil Salinity in the Musaib Area in Central Iraq

Ahmad S. Mhaimeed[1], Weicheng WU[2], Waleed M. AL-Shafie[3], Feras Ziadat[2], Hassan H. Al-Musawi, Kasim A. Saliem[3]

[1] College of Agriculture, Baghdad University, Iraq
[2] International Center for Agricultural Research in the Dry Areas (ICARDA), Amman, Jordan
[3] Ministry of Agriculture (MoA), Baghdad, Iraq

KEYWORDS: Salinity, remote sensing, models, mapping, Iraq

ABSTRACT

Salinity has constituted one of the major problematic issues for agricultural production in Iraq. It is hence essential to develop some rational and reliable approach to conduct salinity mapping and assessment. Recently, we have proposed an innovative methodology in the Dujaila site for this purpose. The aim of this study is to ascertain whether the methodology we developed can be extended to other similar environment taking the Musaib site, another project site in Central Iraq, as an example. Field survey including soil sampling, EM38 (Geonics Ltd.) measurement and land use investigation was conducted and 30 soils samples were analysed in laboratory; 17 Landsat ETM+ spring and summer imagery in the frame of 168-37 from 2009 to 2012 were prepared for the study. By following the same procedure as we have done for the Dujaila site, we obtained similar remote sensing models in the vegetated area, that is, the field measured salinity are functions of the multiyear maximal GDVI (Generalized Difference Vegetation Index). For the non-vegetated area, only land surface temperature (T) among all non-vegetation indices (NVIs) was finally retained in the models, which are slightly different from those in Dujaila. However, these models can predict salinity with high reliability (83%). It is therefore concluded that our methodology developed in Dujaila is operational and extendible to other similar environment for salinity mapping.

INTRODUCTION

Salinization is one of the most active land degradation phenomena in central and southern Iraq. It is estimated that approximately 60% of the cultivated land has been seriously affected by salinity; and 20-30% has been abandoned (FAO, 2011); even in the non-abandoned agricultural land the yield has declined by 30-60% as a consequence of salinization. It is clear that the arable agricultural land would be further reduced because of such land degradation, and might be exacerbated by climate change; the ensuing food security would face harsh challenge in the country. It is hence of pressing importance to quantify the salt-affected soils and ascertain their change trend in space and time in order to provide relevant reference and advice for the local and central governments for decision-making in future agriculture development.

Salinity mapping and assessment are usually conducted by soil survey and interpolation of analytical samples. Whereas with the development of the geospatial technology including remote sensing, GIS, GPS and spatial analysis in the recent decades, a significant progress has been made in this field. Since 1970s, a number of authors namely Hunt et al. (1972), Steven et al. (1992), Mougenot (1993), Rao et al. (1995), Metternicht (1998), Metternicht and Zinck (2003), Brunner et el. 2007, Furby et al. (2010), and so on have investigated soil surface spectral features related to different types of salinity, and resulted that, for example, soil salinity is strongly associated with vegetation indices (VIs). These studies illustrate the advantage, feasibility and great potential of remote sensing but also the problematic issues such as insensitivity of spectral reflectance to low salinity soils (e.g. < 15%, Meugenot, 1993), underestimation of salinity caused by halophyte and salt-tolerant crops such as alfalfa, barley and

cotton (Rao et al 1995, Metternicht and Zinck 2003), and by soil moisture, and also possibly false alarm of salinity due to crop rotation/fallow practice.

In front of these challenges, we have proposed an integrated multiyear maxima-based modelling approach for salinity mapping and assessment in Dujaila in central Iraq. The main objective of this study is to investigate whether the proposed methodology is extendible to other similar area for salinity mapping. Hence, the Musaib area, another important irrigation project area in Mesopotamia, was selected for this purpose. A multitemporal remote sensing dataset and ground measurement data were acquired for this study.

MATERIAL AND METHODS

Study site

The Musaib agriculture project area is located in central Iraq between the Tigris and the Euphrates Rivers, and administratively in the Babylon Governorate (Figure 1). The study site was used for small grain production including wheat, barley, corn and some vegetable crops. The total area of the project is around 250000 ha. The dominant soil types are Aridisols and Entisols with texture class ranging from silt clay loam to silt loam with more than 20 % of lime. Most of the soils are slightly saline to moderately saline, e.g. from 4 to 20 dS/m (MoWR, 1994).

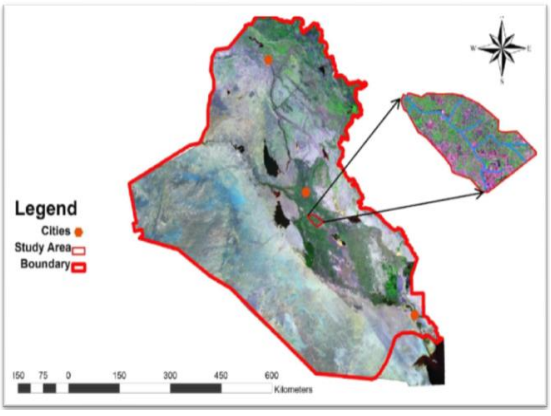

Figure 1: Location of the study area, Musaib

As for climate, Musaib site belongs to subtropical area, characterized by short cool winter and long hot summer. Rainfall is concentrated in winter and spring from November to March with average annual rainfall of about 82.5 mm in the past 60 years (in the adjacent station, Hilla). Winter is cool and short with mean temperature of 18.5°C from December to February. Summer is dry and hot to extremely hot with maximum mean temperature of 46. 5°C in July and August.

Field investigation and data

Field work was conducted in the period from September 2011 to July 2012 including soil sampling, measurement of EM38-MK2 (briefed as EM38, an electromagnetic instrument made by Geonics Ltd to measure soil electrical conductivity), and land use/cover investigation. Soil samples were taken from 30 sites including 17 surface soil samples, 7 profiles and 6 auger holes. Soil electrical conductivity (EC) for all soil samples were determined using EC(1:1 dilution)EM38 readings were conducted in two campaigns: one was in spring (March-April, 45 vertical and horizontal readings) and the other was in early summer (in June-July, when dry season started after harvesting, 23 pairs of readings) in 2012. As designed, both vertical and horizontal EM38 readings were taken in the plots (1×1 m^2), distributed at the three corners of a triangle with a distance of about 15-20 m from each other. The averaged value was regarded as the representative of the observation point in the center of the triangle. The objective of such averaging is to have more comparability between field sampling and satellite images (with pixel size of 30 m). In total, 68 pairs of EM38 readings were made available for this study.

To investigate the extendibility of the methodology we have proposed in Dujaila and develop the properly operational mapping approach in Musaib by remote sensing, a set of Landsat images in the frame of 167-38 were acquired (Table 1).

Landsat Frame: 168-37					
2010 (2009-2012) Landsat7 ETM+		2000 (1998-2002) Landsat7ETM+ and 5TM		1990 (1988-1993) Landsat 5 and 4TM	
Spring	Summer	Spring	Summer	Spring	Summer
2009-03-17	2008-08-05	1999-02-26	1998-08-02	1990-03-29	1989-08-01
2009-04-18	2010-08-11	1999-03-14	2000-08-23	1991-02-12	1990-08-12
2010-03-20	2011-08-14	2000-04-09	2000-08-31	1993-02-17	1990-08-20
2011-02-03	2012-08-16	2000-04-25	2001-08-18		1992-08-19
2011-02-19	2012-09-01	2001-02-23	2002-08-05		
2012-02-22		2001-03-11			
2012-03-09		2001-03-27			
2012-04-26		2001-04-28			
		2002-04-15			

Table 1: Landsat images used in the study

Processing procedure

As we have been aware, a number of vegetation and non-vegetation indices such as NDVI (Normalized Difference Vegetation Index, Rouse et al 1973), EVI (Enhanced Vegetation Index, Huete et al. 1997) are to certain extent sensitive to salinity (Zhang et al. 1997, Garcia et al. 2000, Al-Khaier 2003, Brunner et al. 2007, Lobell et al. 2010); thermal band which can be used for derivation of surface temperature is also of great potential for salinity mapping (Metternicht and Zinck, 1996 and 2003, Goossens and Van Ranst, 1998, and Igbal 2011). All these remote sensing indicators will be produced as we have done for the Dujaila site by the following procedure.

As the first step, atmospheric correction was undertaken for all Landsat imagery using FLAASH model (Perkins et al. 2005) followed by a multispectral transformation to derive the relevant VIs that have been already used by other authors or might be efficient for salinity assessment such as NDVI, EVI, SAVI (Soil Adjusted Vegetation Index, Huete 1988) and SARVI (Soil Adjusted and Atmospherically Resistant Vegetation Index, Kauffmann and Tanre 1992). A new vegetation index developed by Wu (2012), GDVI (of n = 2), which was claimed more sensitive to dryland biomes than other indices, was also derived. The formulae of all these indices are shown in Table 2. Then, the non-vegetation indices (NVIs) such as Tasseled Cap Brightness (BRT, Crist and Cicone 1984, Huang et al. 2002), Principal Components (PCs, especially first three components denoted as PC1, PC2 and PC3), NDII (Normalized Difference Infrared Index, Hardisky et al. 1983, formula see

Index	Full Name	Formula	References
NDVI	Normalized Difference Vegetation Index	$\frac{(\rho_{NIR}-\rho_R)}{(\rho_{NIR}+\rho_R)}$	Rouse et al.(1973)
SAVI	Soil-Adjusted Vegetation Index	$\frac{(1+L)(\rho_{NIR}-\rho_R)}{(\rho_{NIR}+\rho_R+L)}$ Low vegetation, L = 1, intermediate, 0.5, and high 0.25	Huete (1988)
SARVI	Soil Adjusted and Atmospherically Resistant Vegetation Index	$\frac{(1+L)(\rho_{NIR}-\rho_{RB})}{(\rho_{NIR}+\rho_{RB}+L)}$ ρ_{RB} is the same as that in ARVI, L is a correction factor similar to those of SAVI	Kaufman and Tanré (1992)
EVI	Enhanced Vegetation Index	$G*\frac{(\rho_{NIR}-\rho_R)}{(\rho_{NIR}+C1*\rho_R-C2*\rho_B+L)}$ ρ_B = reflectance of blue band, G = 2.5, C1 = 6, C2 =7.5 and L = 1	Huete et al.(1997)
NDII	Normalized Difference Infrared Index	$\frac{(\rho_{NIR}-\rho_{MIR})}{(\rho_{NIR}+\rho_{MIR})}$	Hardisky et al. (1983)
GDVI	Generalized Difference Vegetation Index	$\frac{\rho_{NIR}^n-\rho_R^n}{\rho_{NIR}^n+\rho_R^n}$ n is power number, an integer of the values of 1, 2, 3, 4... n.	Wu (2012)

Table 2: Formulae of the vegetation indices

Note: ρ_{NIR} and ρ_R are respectively reflectance of the near infrared (NIR) and red (R) bands; ρ_B and ρ_{MIR} are respectively that of the blue band and the middle infrared band (e.g. TM band 5)

Table 2) were produced from each spring Landsat image. Land surface temperature (T) was derived from the spring images during the crop growing period (before mid-April). The T was converted from the thermal band of Landsat TM and ETM+ images using the following equations (Chander et al. 2009):

$$L_\lambda = G_{rescale} * Q_{cal} + B_{rescale} \quad (1)$$

$$T = K_2 / \ln((K_1/L_\lambda)+1) \quad (2)$$

Where L_λ – Spectral radiance at the sensor's aperture [W/(m^2 sr µm)]; Q_{cal} – Quantized calibrated pixel value in digital number [DN]; $G_{rescale}$ – Band-specific rescaling gain factor [(W/(m^2 sr µm))/ DN]; $B_{rescale}$ – Band-specific rescaling bias factor [W/(m^{2}sr µm)]; K_1 and K_2 are calibration coefficients. Their values are listed in Table 3.

Factors	Landsat 4 TM	Landsat 5 TM	Landsat 7 ETM+	
			Low Gain	High Gain
$G_{rescale}$	0.055376	0.055376	0.067087	0.037205
$B_{rescale}$	1.2378	1.18	-0.07	3.16
K_1	671.62	607.76	666.09	
K_2	1284.30	1260.56	1282.71	

Table 3: Rescaling factors and calibration coefficients of the Landsat thermal band Note: Extracted from Chander et al. (2009).

A multiyear VI dataset was composed using the same vegetation index (e.g. NDVI) in the period 2009-2012 including both spring and summer images; the same was processed for other VIs (such as EVI, SAVI, ARVI, GDVI) and NVIs (e.g. BRT, PCs and T).

Then, the maximization procedure, i.e., to extract the maximal value of the same VI in each pixel during the observed period 2009-2012, was applied to all VIs and NVIs. The aim of this maximization processing is to avoid the gap problem in recent Landsat ETM+ imagery (after 2003), to remove the possible influences from crop rotation/fallow in the vegetated area and the impacts of soil moisture in the non-vegetated area.

The division of vegetated and non-vegetated areas was realized by thresholding technique using the multiyear maximal NDVI, of which the threshold was set 0.27 after a careful check in the multiband composites of Landsat images. More concretely, when NDVI < 0.27, it is non-vegetated area, otherwise, it is vegetated area.

The maximum remote sensing indicators, e.g. the maximal VIs and NVIs, were linked to the field measured salinity (EM38 readings and laboratory analytical results, EC) using least-square multiple linear regression models at the confidence level of 95% to derive remote sensing salinity models. In operation, VIs were coupled with salinity measurements in the vegetated area and NVIs were linked to salinity in the non-vegetated area to get salinity models respectively for the vegetated area (croplands) and non-vegetated area.

It is worthy of attention that T and NDII have both vegetation and non-vegetation characters, were hence incorporated in salinity modeling for both vegetated and non-vegetated areas.After evaluation of the reliability by linking the modeled salinity to the ground measured data, the salinity models were applied respectively back to the maximum VIs and NVIs of the recent state 2010 (2009-2012), the historical states 2000 (1998-2002), and 1990 (1989-1993) to produce multitemporal salinity maps in which vegetated and non-vegetated areas were mosaicked together.

RESULTS AND DISCUSSION

Salinity models and their reliability

By following the above procedure, the correlation coefficients between VIs/NVIs and salinity (EM38 readings) and the models obtained for the Musaib site are listed in Tables 4 and 5. It is seen clearly that among the all vegetation indices GDVI is, the same as in the Dujaila site, the best salinity indicator for the vegetated area. For the non-vegetated area, the maximum land surface temperature (T) during the crop growing period, and PC1 are good indicators and only T was finally retained in the models (Table 5). This is different from those obtained in Dujaila.

We have to mention that during the VIs/NVIs and salinity coupling analysis, the laboratory measured EC in 2011 and EM38 measurements in spring (March-April) 2012 did not show any reasonable correlation with vegetation and non-vegetation indices, probably due to the fact that the soil samples were taken too close to the roads without enveloping the diversity of crops and covering the different types of bareland, or when EM38 readings were made the land was not dry enough after rainfall events. Fortunately, those obtained during the supplemental sampling campaign in June-July 2012 (dry season after harvesting), show excellent correlations with the vegetation and non-vegetation indices (Table 4) in which we considered the vegetated and non-vegetated areas as an entirety. These samples, in total 23 pairs of EM38 readings, were used for integrated salinity modelling by removing one falling in the gap and the other with non-zeroing problem (i.e. background value could not be adjusted to zero) before measurement was conducted.

	SAVI	GDVI	EVI	T	NDVI	NDII45	PC1	PC2	PC3	TC_BRT
EM_V	-0.820	-0.901	-0.843	0.859	-0.843	-0.692	0.749	0.559	0.548	0.586
EM_H	-0.798	-0.875	-0.821	0.844	-0.821	-0.685	0.737	0.527	0.614	0.576

Table 4: intergrated correlations between EM38 readings and Vis/NVIs in Musaib

Type	Equations	Error scope	Multiple R^2
Vegetated area	EM_V = -824.134 + 918.536*GDVI - 754.204*ln(GDVI)	± 41.700	0.925
	EM_H = -606.197 – 460.043*ln(GDVI) + 245.086*Exp(GDVI)	± 48.559	0.862
Non-Vegetated area	EM_V = 2570683.24 + 1821.24T – 546476.07*ln(T)	± 62.944	0.829
	EM_H = 2608853.46 + 1842.4T – 554286.69*ln(T)	± 51.217	0.846

Table 5: Integrated salinity models

Note: 1) Models were obtained with 21 samples recoded in the supplemental sampling campaign in the dry season June-July 2012 and one outliner was removed; 2) EM_V and EM_H are respectively vertical and horizontal readings of EM38; T is the maximum surface temperature during the growing period (February-mid April) in K; 3) EM_V/EM_H can be converted into electrical conductivity (EC in dS/m) by the following relationships obtained from the regional transect sampling and measurement in Mesopotamia: $EC = 0.0005EM_V^2 - 0.0779EM_V + 12.655$ ($R^2 = 0.850$), and $EC = 0.0002EM_H^2 + 0.0956EM_H + 0.0688$ ($R^2 = 0.791$).

To evaluate their reliability, the developed models were applied back to the multiyear maximum GDVI and T of 2009-2012 to produce the salinity maps respectively for the vegetated and non-vegetated areas. After mosaic, the integrated salinity map was derived and checked against the ground measured salinity by least-square linear regression analysis. It is found that the agreement between the predicted and field measured is very high (R^2 = 0.83, Figure 2). This means that the models have high predictability and reliability, about 83%.

Some researchers may concern about the reasonability of the models that involved T. It is a common knowledge that thermal conductivity of materials is temperature (T) dependent, and the former is associated with electrical conductivity (EC). Abu-Hamdeh and Reeder (2000) have ascertained the relationship between thermal conductivity and salinity, that is, thermal conductivity decreases with an increase in the amount of added salts at given moisture content. Sepaskhah and Boersma (1979) found that the apparent thermal conductivity is independent of water content at very low water contents. Consequently, in driest condition (lowest moisture) as in our case after maximization, thermal conductivity is associated with the salt amount – salinity at the given soil texture and bulk density. Therefore, we believe that T-related models are relevant for non-vegetated area.

Salinity maps

The evaluated models, EM_V-GDVI and EM_H-T, were respectively applied to the historical maximum GDVI and T for salinity mapping in the vegetated and non-vegetated areas. After mosaicking, the multitemporal salinity maps were produced and presented in Figure 3.

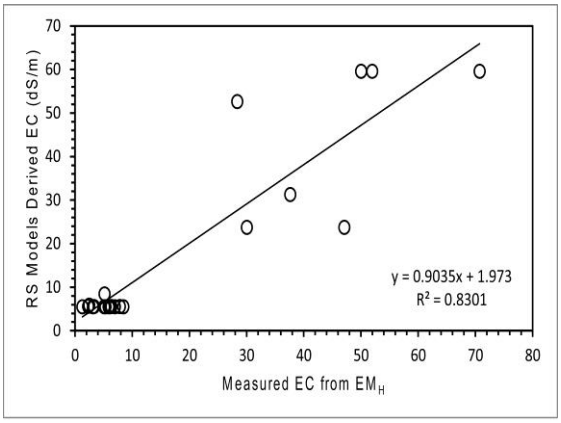

Figure 2: Accuracy of the mosaicked salinity maps of 2010 again the ground measured data in Musaib

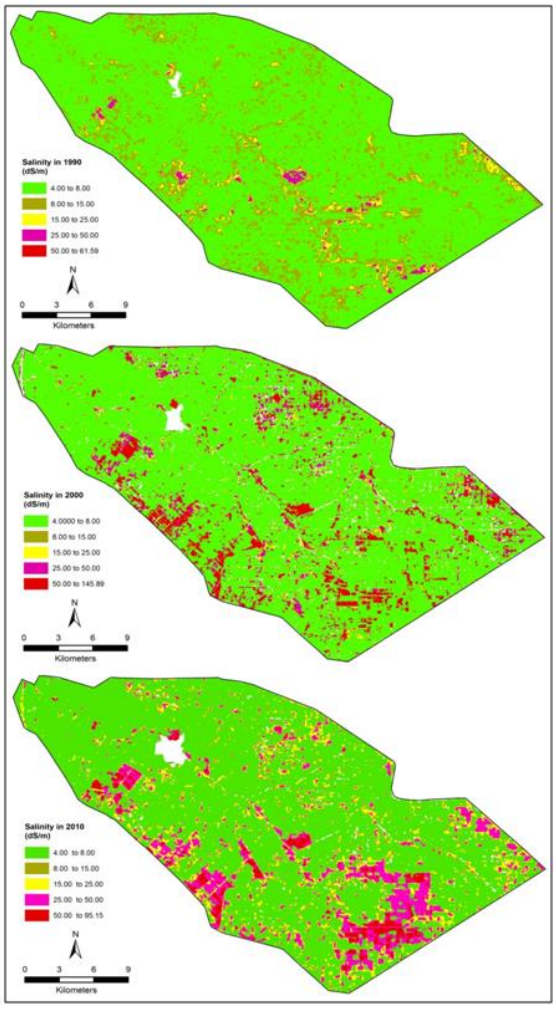

Figure 3: Multiemporal salinity maps of the Musaib pilot site

The salinity in the cultivated areas is mostly in a range of 0-8 dS/m (dark green and green). Salts only get gathered in certain drainage ditches, non-reclaimed areas and abandoned cropland transported by drainage system or due to damage of the irrigation/drainage system or left by dry-up of logged salty water (see magenta and red colour, salinity > 25 dS/m). These multitemporal show clear change in salinity in space and time.

CONCLUSION

This study demonstrates that through similar processing procedure as we have done for Dujaila it is possible to develop similar but proper models for salinity mapping and assessment in the Musaib site.

To our expectation, the map of the present state derived from the newly developed salinity models is agreed well with the field measurement in Musaib; and this implies that the models developed are operational and these maps can be used for further salinity change trend tracking and quantification so as to provide advice for local governments and farmers to plan future agriculture development. So we concluded that the methodology we proposed in Dujaila is operational and extendable to other similar environment for salinity quantification and assessment.

Acknowledgements

The study is funded by ACIAR [Project No: LWR/2009/034]. All Landsat images were freely obtained from the USGS data server: http://glovis.usgs.gov/

REFERENCES

Abood, S., Maclean, A. and Falkowski, M., 2011. Soil salinity detection in the Mesopotamian agricultural plain utilizing WorldView-2 Imagery. Available at: http://dgl.us.neolane.net/res/img/16bb89b080930a8ad1fdfc17665883e9.pdf

Abu-Hamdeh, N. H., Reeder, R. C., 2000. Soil thermal conductivity effects of density, moisture, salt concentration, and organic matter. Soil Science Society of America Journal (SSSAJ) 64, 1285-1290 (doi:10.2136/sssaj2000.6441285x).

Al-Khair, F., 2003. Soil salinity detection using satellite remote sensing. Ms Thesis, ITC International Institute for Geo-information Science and Earth Observation. The Netherlands.

Brunner, P., Li, H.T., Kinzelbach, W. and Li, W.P., 2007. Generating soil electrical conductivity maps at regional level by integrating measurements on the ground and remote sensing data.

Chander, G., Markham, B.L., Helder, D.L., 2009. Summary of current radiometric calibration coefficients for Landsat MSS, TM, ETM+, and EO-1

ALI sensors. Remote Sensing of Environment 113, 893–903.

Crist, E. P., Cicone, R. C., 1984. Application of the Tasseled Cap concept to simulated Thematic Mapper data. Photogrammetric Engineering and Remote Sensing 50, 343-352.

FAO, 2011. Country pasture/forage resource profiles: Iraq. FAO, Rome, Italy, p.34.

Furby, S. Caccetta, P. and Wallace, J., 2010. Salinity monitoring in Western Australia using remotely sensed and other spatial data. Journal of Environmental Quality 39, 16–25.

Garcia, L., Eldeiry, A. and Elhaddad, A., 2000. Estimating soil salinity using remote sensing data. Civil Engineering 1994, 1-10.

Goossens, R. and Van Ranst, E., 1998. The use of remote sensing to map gypsiferous soils in the Ismailia Province (Egypt). Geoderma 87, 47–56.

Hardisky, M. A., Klemas, V. and Smart, R. M., 1983. The influences of soil salinity, growth form, and leaf moisture on the spectral reflectance of Spartina alterniflora canopies. Photogrammetric Engineering & Remote Sensing 49, 77-83.

Hunt, G., Salisbury, J. and Lenhoff, C., 1972. Visible and near infrared spectra of minerals and rocks: V. Halides, phosphates, arsenates, venadates and borates. Modern Geology 3, 121– 132.

Huete, A. R., 1988. A soil adjusted vegetation index (SAVI). Remote Sensing of Environment 25, 295–309.

Huete, A. R., Liu, H. Q., Batchily, K., and van Leeuwen, W., 1997. A comparison of vegetation indices global set of TM images for EOS-MODIS. Remote Sensing of Environment 59, 440-451

Huang, C., Wylie, B., Yang, L., Homer, C., Zylstra, G., 2002. Derivation of a tasseled cap transformation based on Landsat 7 at-satellite reflectance. International Journal of Remote Sensing 23,1741–1748.

Iqbal, F. 2011. Detection of salt affected soil in rice-wheat area using satellite image. African Journal of Agricultural Research 6, 4973-4982.

Kaufman, Y. J. and Tanré, D., 1992. Atmospherically resistant vegetation index (ARVI) for EOS-MODIS. IEEE Transactions on Geoscience and Remote Sensing 30, 261-270.

Lobell, D. B, Lesch, S. M. and Corwin, D. L., Ulmer, M. G., Anderson, K. A., Potts, D. J. , - -- - Doolittle, J. A., Matos, M. R. and Baltes, M. J., 2010. Regional-scale assessment of soil salinity in the red river valley using multi-year MODIS EVI and NDVI. Journal of Environmental Quality 39, 35–41.

Metternicht, G., 1998. Analysing the relationship between ground based reflectance and environmental indicators of salinity processes in the Cochabamba Valleys (Bolivia). International Journal of Ecology and Environmental Sciences 24, 359– 370.

Metternicht, G.I. and Zinck, J.A., 2003. Remote sensing of soil salinity: potentials and constraints, Remote Sensing of Environment 85, 1 –20.

Mougenot, B., Pouget, M. and Epema, G., 1993. Remote sensing of salt-affected soils. Remote Sensing Reviews 7, 241–259.

MoWR.1994.Soil Map for all Iraq: Baghdad and Babelon Governments.

Perkins, T., Adler-Golden, S., Matthew, M., Berk, A., Anderson, G., Gardner, J. and Felde, G., 2005. Retrieval of atmospheric properties from hyper and multispectral imagery with the FLAASH atmospheric correction algorithm. In: Schäfer, K., Comerón, A.T., Slusser, J. R., Picard, R. H.,

Rao, B., Sankar, T., Dwivedi, R., Thammappa, S., Venkataratnam, L.,Sharma, R. and Das, S., 1995. Spectral behaviour of salt-affected soils. International Journal of Remote Sensing 16, 2125–2136.

Rouse, J. W., Haas, R. H., Schell, J. A. and Deering, D. W., 1973. Monitoring vegetation systems in the Great Plains with ERTS. In: Proceedings of the Third ERTS-1 Symposium, NASA SP-351, 1, 309-317.

Steven, M.D., Malthus, T.J., Jaggard, F.M. and Andrieu, B., 1992. Monitoring responses of vegetation to stress. In: Cracknell A.P. and Vaughan, R.A. (Eds). Remote sensing from research to operation: Proceedings of the 18th Annual Conference of the Remote Sensing Society. United Kingdom.

Wu, W., 2012. The generalized difference vegetation index (GDVI) for land characterization. Abstract collected in the Proceedings of the 8th ISSC (International Soil Science Congress), Volume III, Izmir, Turkey, May 15-17, 2012 (http://soilcongress.ege.edu.tr/files/books/Volume3.pdf). Full paper submitted to Remote Sensing in 2013 (under review).

Zhang, M., Ustin, S., Rejmankova, E. and Sanderson, E., 1997. Monitoring Pacific coast salt marshes using remote sensing. Ecological Applications 7, 1039– 1053.